Investigation of Tribological Behaviour of a-C:H Coatings for Dry Deep Drawing of Aluminium Alloys

R. Zhao[1*], J. Steiner[2], K. Andreas[2], M. Merklein[2], S. Tremmel[1]

[1]*Institute of Engineering Design, Department Mechanical Engineering, Friedrich-Alexander-Universität Erlangen-Nürnberg(FAU), Martensstraße 9, 91058 Erlangen, Germany.*
[2]*Institute of Manufacturing Technology, Department Mechanical Engineering, Friedrich-Alexander-Universität Erlangen-Nürnberg (FAU), Egerlandstraße 13, 91058 Erlangen, Germany.*

Abstract

Lubricant-free sheet metal forming increases resource efficiency and contributes to environmental protection. One approach to reduce friction and wear in dry forming is a tool-sided application of carbon based coatings. In this work, amorphous hydrogenated carbon (a-C:H) coatings were prepared by plasma-enhanced chemical vapour deposition (PECVD). The coating samples were deposited under different amounts and ratios of acetylene (C_2H_2) and argon (Ar) gas atmospheres. The studied total gas mixtures covered the range of 200 to 300 sccm. The ratios of C_2H_2 to Ar varied from 1:1 to 5:1. The coatings samples were characterized regarding their coating thickness, roughness and mechanical as well as chemical bonds structures. Raman spectra with Nd-YAG laser of 532 nm was used to estimate the ratios of sp^3 fractions in the a-C:H coating samples. The tribological behaviour was investigated under lubricant-free conditions using a ring-on-disc tribometer. As counter bodies, two aluminium alloys commonly used in industrial applications were selected. Laser scanning microscope (LSM) analyses were conducted on coating surfaces before and after tribological tests. The relationships between chemical bonds compositions and coating properties were clarified. Their tribological performances against aluminium alloys were investigated using ring-on-disc tribometer. Finally, one a-C:H coating variant with promising tribological performance against aluminium alloys was exemplarily tested in a flat strip drawing test, which models the tribological conditions in the flange area of a deep drawing process.
Keywords: Dry sheet metal forming, DLC, aluminium, adhesive wear

*Corresponding author: Rong Zhao (zhao@mfk.fau.de).

1. INTRODUCTION

The enhanced environmental awareness and limited global fossil resources motivate improvement of ecological efficiency of forming processes with minimal lubricant usage [1]. The lubricant-free production processes have a number of ecological and economic benefits. Besides the abandonment of lubricants with environmentally hazardous substance, expensive costs for removing the remained lubricant from the formed workpiece are saved. However, achieving a lubricant-free forming process for mass production faces many challenges. Due to direct contact between workpiece and tool adhesive wear on the forming tool surface becomes a significant problem. As a consequence of accumulative transferred material, the surface quality of the finished workpieces is reduced and at the same time tool life is reduced.

Adhesion is one of the four representative wear types. It comes from directly contact of two boundary surfaces [2]. Unlike abrasion and surface disruption, which result from mechanical contact, adhesion is more initiated by interactions of materials on atomic and molecule level [3]. In case of adhesion, the atoms on both boundary surfaces are primarily bonded due to chemical interactions with oxygen in the air and Van der Waals force resulted from atomic electrostatic interactions [4]. According to BOWDEN und TABOR [5], the bonds are after short-term cold welding immediately broken up due to sliding movement. The necessary force or energy to damage these cold-welded bonds are primarily responsible for the friction in case of adhesive wear [2]. Many works have reported about the outstanding tribological properties of amorphous carbons coatings, also called diamond-like carbon (DLC). Because of its unique carbon network the coating combines advantages both from diamond and graphite. The amorphous carbon coatings can be prepared by wide range of techniques. Among them, the plasma-enhanced chemical vapour deposition (PECVD) in acetylene or methane/hydrogen gas atmosphere [6] is one of the most common used methods. According to

HETZNER *et al*. [7], the tungsten doped amorphous carbon coating variants (a-C:H:W) showed their potentiality for sheet bulk metal forming processes, even under boundary lubrication and mixed lubrication conditions. It was reported in [8] that the a-C:H:W coating on the forming tool surface can reduce the adhesive wear against steel sheet. In [9] the tribological behavior of DLC coatings applied to steel sheet-forming tools under process relevant conditions are shown. The tetrahedral hydrogen free amorphous carbon coating system (ta-C) used on deep drawing dies showed good anti-wear property [10]. A lower friction of ta-C against aluminum sheet during sliding processes without lubricant was reported [8]. This is due to its high hardness and lower adhesion tendency to aluminum based light metals in comparison to other carbon coating types [11].

The coefficients of friction in the majority of studies on amorphous carbon coatings are measured by the ball-on-disc setup. It involves a circular point contact. However, tribological behavior in area contacts has been reported rarely. The applied methodology in this paper is shown in Figure 1. The relationship between deposition parameters and coating properties will be clarified. The tribological behaviors of each coating against two aluminum alloys (AA5182 and AA6014) were investigated by a ring-on-disc tribometer in area contacts. Wear mechanisms that are responsible for the observed friction behaviour of a-C:H coatings is explored. A more process-like flat strip drawing test of one promising a-C:H coating variation is conducted to evaluate the application potential in sheet metal forming.

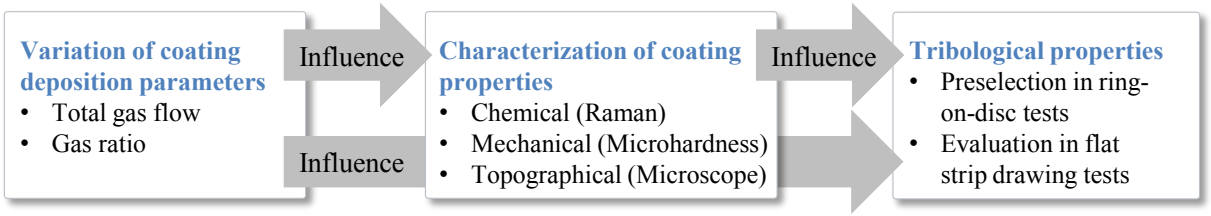

Figure 1: *Methodology for evaluation of the tribological behaviour of a–C:H coatings against aluminium alloys.*

2. EXPERIMENTAL SETUP

2.1 Coating deposition

The a-C:H coatings were deposited on tool steel 1.2379 (X155CrVMo12,). The steel substrates were ring shaped with inner and outer diameter of 10 and 20 mm, respectively. All the characteristic measurements were conducted on samples deposited on polished discs (Ø25x5 mm) with $R_z \leq 0.2$ µm and $R_{pk} \leq 0.01$ µm to avoid measurements with high standard deviations. Prior to coating, the substrates were hardened to HRC 60 ± 1. The annealing process of the steel substrate was carried out at a temperature, which was higher than the actual coating temperature. So that no microstructure changes in steel occur during the coating processes. Such hardening process ensures stable mechanical properties of the substrate during the whole coating process. The ring-shaped substrate surfaces were lapped and polished to a roughness of $R_z = 0.9 \pm 0.1$ µm and $R_{pk} = 0.1 \pm 0.01$ µm, which represents the surface qualities of conventional deep drawing tools.

The a-C:H coatings were deposited using a hybrid PVD/PECVD coating machine (H-O-T, TT-300) with a twofold rotating charging rack. The basic coating system consists of a Cr adhesive layer, a WC interlayer, a-C:H:W interlayer and the a-C:H functional layer. For the Cr adhesive layer and the WC interlayer arc evaporation and unbalanced magnetron sputtering were used as coating technologies, respectively. The a-C:H coating functional layer was deposited by PECVD using C_2H_2 as precursor gas. There are many factors that can affect the final features of a a-C:H coating, from precursor gas C_2H_2, sputter gas Ar, substrate bias voltage, reactor temperature, to previous etching, heating processes and even contaminations in the reactor. The substrate bias voltage U_{bias} is well known to have great impact on coating growth structure and hardness. [12] TILLMANN *et al.* reported in [13] that with increasing bias voltage the hydrogen content in the a-C:H coating decreases and hardness increases as U_{bias} varied from -75 to -200 V. Under high substrate bias U_{bias} the charged atoms or particles in the reactor become high kinetic energetic. With increasing atomic energy the compressive stress rises quickly and reaches its maximum if the impact energy is 20 eV per atom [14]. This leads to poor adhesion of coating to substrate and premature failure during application. In addition, an excessively high bias makes the energetic atoms preferably to bombard the surface, which destroys the grown coating structure. Furthermore, frequently bombardment has also great uncontrolled thermal effect to

the substrates, *e.g.* deposition process with substrate bias of -1200 V leads to substrate self-heating to 160-170°C, without any external heating system. The applied PVD-/PECVD- coating machine in this work is able to regulate substrate bias up to -1200 V. However, during a deposition process with U_{bias} higher than -550 V no a-C:H coating formation was observed on polished steel. The reasons are, as mentioned before, the strongly bombardment and thus destroy of a-C:H:W adhesive layer. The investigated substrate bias voltage U_{bias} was kept constant at -550 V. This option is based on the premise that, a complete a-C:H coating system can be prepared with acceptable adhesion and hardness as high as possible. Many studies have reported the influence of deposition temperature on coating properties. SATTEL *et al.* [15] and FADZILAH *et al*. [16] have reported that a reduction of deposition temperature leads to increasing of the sp^3 configuration, density and compressive stress of a-C:H coatings. It was reported in [17] that the a-C:H coatings were prepared at room temperature. Considering the self-heating effect resulted from atoms and particles bombardments on substrate surface at U_{bias}=-550V, a temperature lower than 80°C in the actual deposition process could not be achieved. In addition, high process temperature improves diffusion during coating growth and lead to relatively low deposition rate. The temperature was kept thus in this case at 80 °C if U_{bias}=-550V. For a coating thickness around 2 µm, the deposition time for all a-C:H functional layers were kept constant for 8 580 s according to general deposition rate of a a-C:H coating in [18]. The admissible C_2H_2 and Ar gas flows in the reactor are 20-290 sccm and 0-500 sccm, respectively. The lowest total gas flow to initiate the glow discharge in reactor of about 300 L is 200 sccm using mid-frequency power supply (40 kHz, pulse width 5µs). A series of a-C:H coatings deposited under gas ratios of Φ(Ar)/Φ(Ar+C_2H_2) from 0 to 70% were investigated in [19]. It was shown, that the a-C:H coatings deposited in the range of Φ(Ar)/ Φ(Ar+C_2H_2) = 10 to 50% had generally linear relationships with coating properties. If the gas mixture is further diluted with Ar, the tendencies of some coating properties associated with gas ratios would be changed, *e.g.* coating compressive stress increases with Ar dilution and reached its maximum if Φ(Ar)/ Φ(Ar+C_2H_2) = 50%; wear rate reached its minimum Φ(Ar)/ Φ(Ar+C_2H_2) = 50%. In this work, the gas flow ratios were varied in the range of Φ(C_2H_2)/ Φ(Ar)=1:1 to 5:1 to prepare coatings with different mechanical properties, which is based on the results of coatings prepared under Φ(Ar)/ Φ(Ar+C_2H_2) = 10 to 50% in [19]. The detailed parameters are shown in Table 1.

Table 1: *Variation of C_2H_2 and Ar flows for deposition of a-C:H coatings*

Sample ID	**Φ(C_2H_2) in sccm**	**Φ(Ar) in sccm**	***Ratio* (C_2H_2 / Ar)**	***Total gas flows* in sccm**
100/100	100	100	1:1	200
150/150	150	150	1:1	300
161/64	161	64	2.5:1	225
188/62	188	62	3:1	250
166/34	166	34	5:1	200
220/40	220	40	5.5:1	260
250/50	250	50	5:1	300

2.2 Coating characterization

After deposition the original a-C:H coating surface was analysed using laser scanning microscope (LSM; Keyence, VK-X 100K). From LSM the topographical appearance of the original coating surface was shown in visual and height information. Prior to tribological tests, ring-shaped coated surface was polished using 1 µm diamond suspension to avoid great material loss. Before and after polishing process the surface roughness was measured. The average distance between the highest peak and lowest valley R_z and the reduced peak height R_{pk} values were characterized by tactile stylus measurements according to DIN EN ISO 4287 [20]. Each measurement was repeated 5 times on the coated surfaces. The interfacial adhesion between the coating and the substrate was measured by scratch test according to DIN EN 1071-3 [21]. Using an optical microscope the normal force L_{c1}, at which the first failure of the coating occurs, was evaluated. The crater grinder method was applied to measure the coating thickness according to DIN EN 1071-2 [21]. Each above-mentioned measurement was repeated 3 times on one sample pro coating variation. Micro hardness of 10 points of the coated surfaces was determined by Vickers indentation (Fischer, FISCHERSCOPE H2000) with indentation force of 10 mN in 10 s according to DIN EN ISO 14577-1 [22]. Raman spectra were acquired from the coatings to investigate the chemical bonds. The applied Raman

spectrometer is equipped with a CCD detector with Nd:YAG laser at 532 nm. The applied laser power was 10 mW to avoid undesired structure changes or even damage of the coating [23].

2.3 Tribological tests

The tribological behaviour of all coating variations was investigated by ring-on-disc tribometer (Wazau, TRM 1000) under lubricant free conditions. The tests were conducted under ambient atmosphere with relative humidity $RH = 43\ \% \pm 2.4\ \%$ at room temperature ($T = 23.2 \pm 0.4$ °C). The tribological system consists of a unidirectional rotating ring and a fixed square aluminium alloys with a dimension of 28x28x1 mm. The ring surface with diverse a-C:H coatings was loaded against the flat square aluminium sheet. Prior to tribological testing the ring and sheet were cleaned with isopropanol. The experiment was repeated three times. The detailed test conditions are described in Figure 2. The tested surfaces were investigated by LSM, especially the areas with adhesive wear, which helps determine wear mechanisms during sliding under lubricant-free conditions in area to area contact.

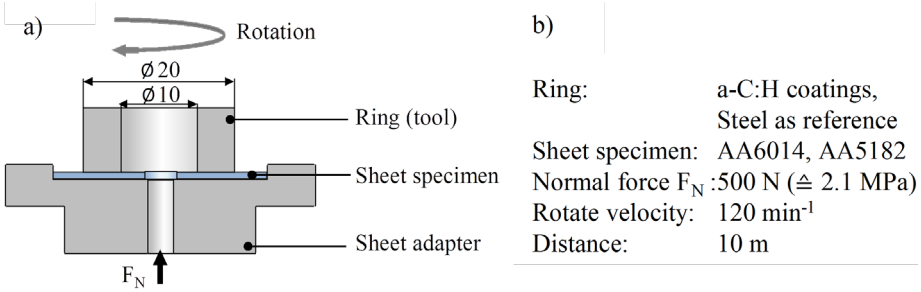

Figure 2: Ring-on-disc tribometer a) test setup [8] and b) test parameters.

The coating variant with the most promising tribological behaviour was additionally tested in plane strip drawing tests. This test setup is commonly used to analyse tribological properties in the flange area of a deep drawing process [24]. Strip drawing tests represent an open tribological system with constantly new sheet material in contact with the tools. Thus, these testing conditions are much closer to the real contact conditions in a sheet metal forming process compared to ring-on-disc tests. However, the tribometer tests are necessary for a first screening of potential surface modifications in a simple test setup. The size of the specimen and the schematically test setup are shown in Figure 3. The strips are cut with a laser to a size of 500 mm x 65 mm. To avoid a contact of the cutting edge with the tool surface, the sheet metal strips are wider than the friction jaws with a size of 100 mm x 55 mm. The sheet metal strip is located between an upper, fixed and a lower, movable friction jaw. By moving upwards the lower friction jaw applies a defined normal force F_N. The strip is clamped on one side and is drawn through the jaws with a constant drawing velocity v_{rel}. The tribological behaviour of coated jaws is investigated under close to real forming conditions. Thus, the relative velocity is set to 100 mm/s and a contact pressure of 3 MPa is applied. Both parameters represent typical conditions in a conventional deep drawing process [24]. During drawing of the strips the drawing force F_{Draw} is recorded. By applying the Coulomb friction law the coefficients of friction are determined by computing the proportion between F_{Draw} and F_N. Because of a two sided contact between sheet material and tools only half of the normal force needs to be considered.

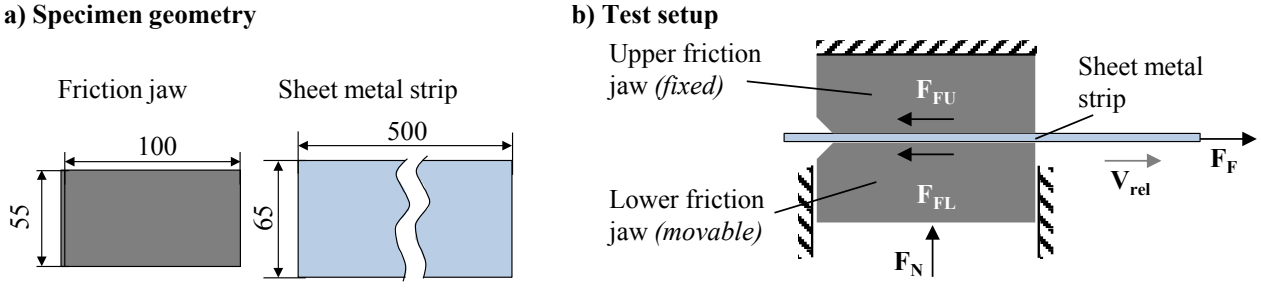

Figure 3: *Flat strip drawing test a) specimen geometry and b) principle test setup.*

3. RESULTS AND DISCUSSION

3.1 Coating Properties

The total thicknesses of the generated coating systems including interlayers are in the range of 1.5 µm to 3.0 µm. The thickness measurements were conducted on original deposited steel disc without polishing. The critical last for the first crack is in the range of 12 N-18 N. More detailed values and mechanical properties are summarized in Table 2. Considering BÜCKLE rule [22], the coatings samples on discs for hardness determining were additionally polished to ensure small deviations.

Table 2: *Coating properties of all a-C:H variations.*

Coating	Thickness	Adhesion	Hardness	Indentation
	t in µm	L_{c1} in N	HV 0.001	E_{IT} in GPa
100/100	1.65±0.07	14.0±2.0	2 087.0±25.2	555.1±11.3
150/150	2.19±0.17	15.0±2.0	1 883.6±187.7	461.5±62.3
161/64	1.77±0.22	15.0±1.0	2 284.8±129.4	606.8±39.9
188/62	2.24±0.01	16.0±2.0	2 031.5±110.1	531.6±26.8
166/34	1.51±0.12	12.0±1.0	2 202.3±92.8	589.3±24.0
220/40	2.34±0.07	18.5±1.0	1 936.8±109.5	502.7±28.9
250/50	2.96±0.08	16.3±0.6	1 922.9±117.4	475.7±30.0
Steel	–	–	642.8 ± 88.2	164.6 ± 16.7

Figure 4 shows LSM images of a representative a-C:H coated surface before and after mechanical post treatment. Figure 4 a) and c) depict that surface asperities due to small particles with height up to 1 µm are distributed on the surface. They result from a large number of macro-particles (the so-called droplets) entrapped in the Cr adhesive layer. As shown in Figure 4 b) and d), after polishing the particles on coating surfaces were removed.

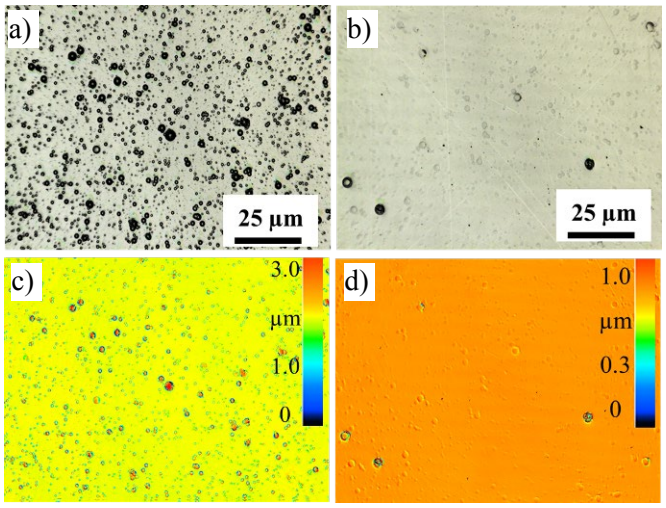

Figure 4: *LSM images of a-C:H coating 220/40 surface a) without and b) after polishing, c), d) height informations.*

The roughness of original coated samples varies from R_z = 1.3 µm–1.6 µm and R_{pk} = 0.29 µm–0.36 µm. The coating samples are mechanical polished for tribological tests to surface quality of R_z = 0.5 µm-0.7 µm and R_{pk} = 0.05 µm-0.07 µm. The detailed values are summarized in Figure 5.

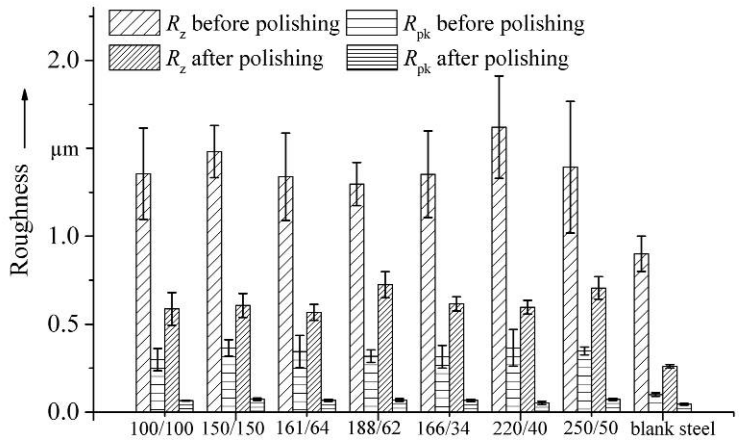

Figure 5: *Surface roughness of the coating samples before and after polishing.*

Main effect [25] plots of the two varied process factors were shown in Figure 6. The differences between level means imply that each factor affects the responses, here coating properties, differently. As shown in Figure 6 a), the deposition rate increases with C_2H_2 concentration if the coatings were deposited under 300 sccm gas flows. The C-H radicals attach more quickly to substrate boundary surface than the other atoms in the reactor [26]. Therefore higher concentration of C_2H_2 accelerates coating growth process. It is also to be seen, that the deposition rate under 200 sccm was very low and almost not affect by gas compositions. Due to low total flows or low pressure in the PECVD reactor, the glow discharge of gasses was undergone with lower current. The ions and radicals in this plasma field gained not enough kinetic energy and thus unbeneficial for coating growth. The effect for adhesion depends strongly on total gas amounts. Hardness and indentation modulus of the coatings are not very pronounced if the big standard deviation is considered.

As shown in Figure 6 b), the deposition rate increases with the process gas amount. A precondition for formation of coating on substrate is the growth of cluster, which makes it possible for further growth steps [29]. The higher amount of total gas atoms in the reactor accelerates the growth of clusters and thus the formation of coatings. The a-C:H coating deposited under higher process pressure has generally better adhesion. However, hardness und indentation modulus decrease with raising gas amounts. The same effect is observed preferably if the total flow increases. According to PUJADA *et al*. [27], the increasing C_2H_2 flow led to reduction of hardness and indentation modulus in the WC doped a-C:H-matrix, as the C_2H_2 amount varied from 0 to 10 sccm. The investigation of [28] shows the same tendency, as the C_2H_2 amount varied from 7 to 49 sccm. In the plasma with low total gas amounts the mean free path of each molecular is longer and thus lead to less energy loss through collision with other species. Ions with high energy promote the formation of sp^3 bonds formations [30], which is well known associated with high hardness and modulus. However, it fits reasonably for sp^3-rich and hardest amorphous carbon coating like ta-C, but less for a-C:H [32]. In the case of a-C:H coatings the hardness and modulus depend more on the form of existed sp^2 bonded carbon atoms, which will be discussed with help of Raman data in the next part.

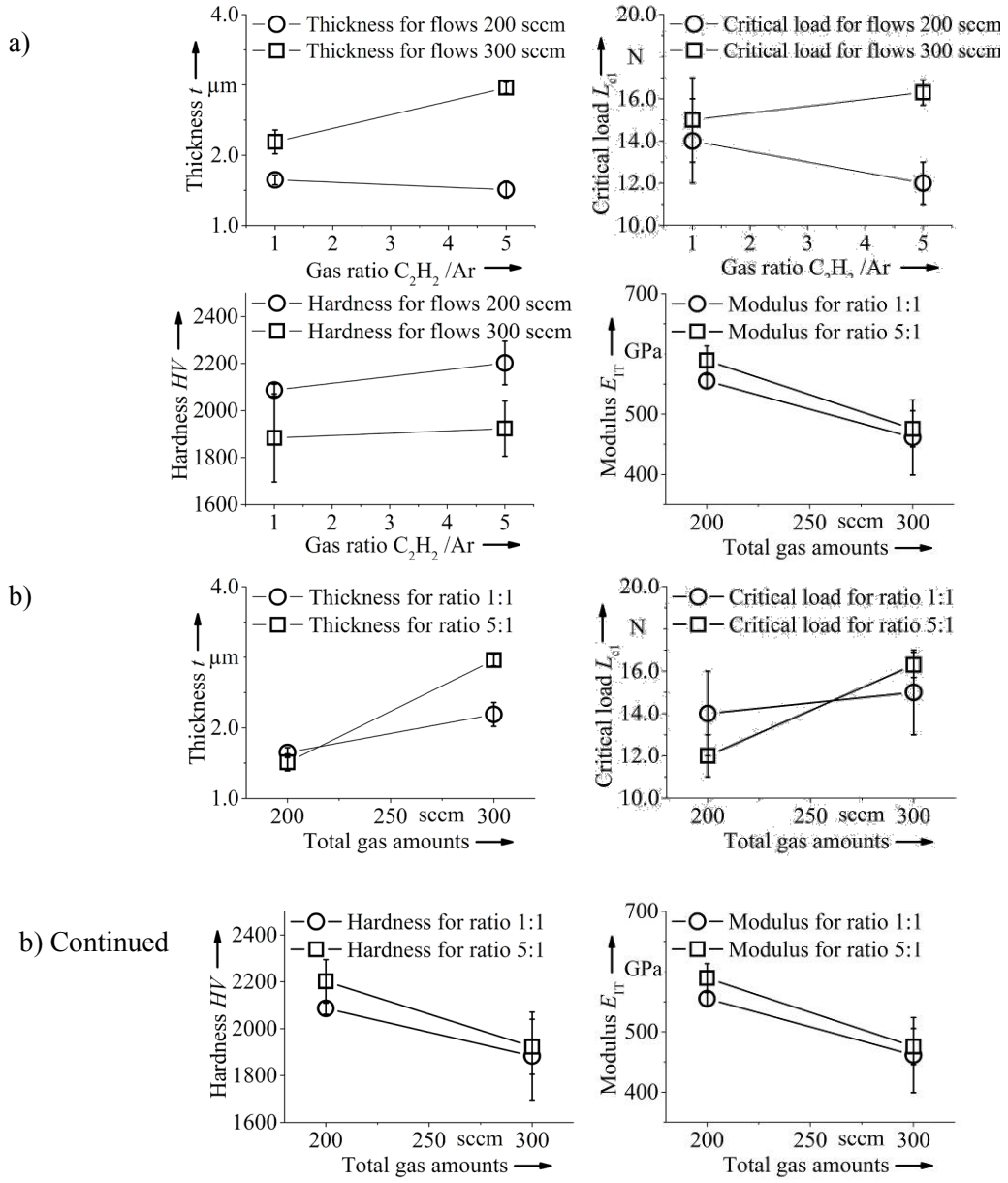

Figure 6: *Main effect size of a) acetylene concentration and b) deposition total gas flows on coating thickness t, critical last of the first crack L_{c1}, Vicker's hardness HV and indentation modulus E_{IT}.*

The Raman spectroscopy measures the inelastic scattering of chemical bonds by laser. Figure 7 a) shows the Raman spectra for all a-C:H coating samples. The Raman analysis was conducted in the range of 800 to 2000 cm^{-1}, since all carbon coatings show their characteristic peaks in this range [30]. The most usually investigated peaks are D peak and G peak, which lie at about 1560 cm^{-1} and 1360 cm^{-1}, respectively, for visible excitation. Both of them describe states of sp^2 bonds. Because the excitation resonates with π states due to its lowest excitation energy. The G peak hats his origin in bond stretching of all pairs of sp^2 atoms in both rings and chains. The D peak describes the breathing modes of sp^2 atoms in rings.

A Raman spectrum is associated with clustering of the sp^2 phase, presence of sp^2 rings or chain and the sp^2/sp^3 ratio [31]. The intensity ratio I_D/I_G indicates the disorder level and sp^3 content in the amorphous graphite phase for the DLC coating, which is also associated to the coating hardness [32]. The peak intensity is fitted by two-curve Gaussian functions. Prior to each fitting a baseline is subtracted from the original curve. The calculation of I_D/I_G ratios in this work was conducted using the data analysis software Origin 9.0. Figure 7 b) shows the peak fit for one coating sample (100/100). The essential results are summarized in Table 3 concerning the deposition process parameters.

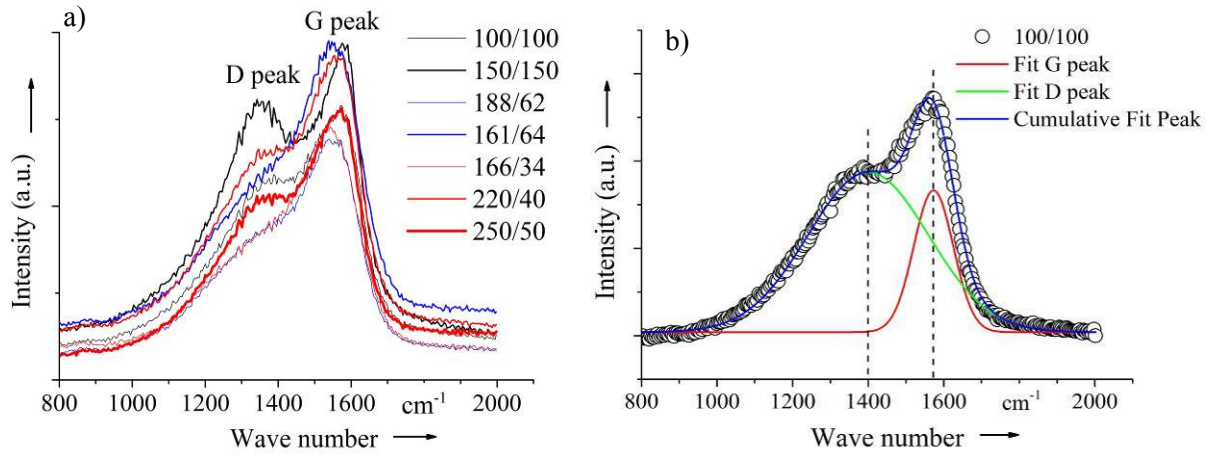

Figure 7: *Raman spectra of a) all a-C:H coatings using 532 nm green laser and b) example for peak fit process using the coating 100/100 Raman spectrum.*

ROBERTSON *et al*. [32], [33] had developed a three-stage model to describe different amorphization states with increasing disorder of sp^2 grains. A G position from 1550 to 1580 cm^{-1} implied that all samples in this work can be considered as a mixture of nanocrystalline graphite and amorphous carbon network in both ring and chain form. According to [33], the sp^3 configuration increases from 0-20 % as the I_D/I_G decreases from 2.0 to 0.25. I_D/I_G ratio higher than 2.0 implies that there is no sp^3 content in the coatings. As shown in Table 3, the coatings 100/100, 188/62, 220/40, 150/150, 250/50 belong to this group. A ratio of 1.70 and 1.87, like the coatings 161/64, 166/63, implies a sp^3 content of about 4-10 %. The precursor gas HC≡CH tends to form unsaturated C-H radicals during deposition process. For formation of more sp^3 bonds additional hydrogen is required.

Table 3: *Raman peak analysis using two Gaussian peaks including information of the peak intensity ratio of D peak und G peaks I_D/I_G, position of D peak $x_c(D)$, position of G peak $x_c(G)$ and full width at half maximum of G peak $FWHM_G$.*

	$\Phi(C_2H_2):\Phi(Ar)$ = 1:1	$\Phi(C_2H_2):\Phi(Ar)$ = 3:1	$\Phi(C_2H_2):\Phi(Ar)$ = 5:1
$\Phi(C_2H_2)+\Phi(Ar)$ = 200 sccm	Coating 100/100 I_D/I_G = 3.44 $x_c(D)$ = 1 400.3 $x_c(G)$ = 1 573.0 $FWHM_G$ = 123.4	Coating 161/64 I_D/I_G = 1.87 $x_c(D)$ = 1 390.6 $x_c(G)$ = 1 560.4 $FWHM_G$ = 154.6	Coating 166/34 I_D/I_G = 1.70 $x_c(D)$ = 1 377.1 x_c G) = 1 550.7 $FWHM_G$ = 159.8
$\Phi(C_2H_2)+\Phi(Ar)$ = 250 sccm	-	Coating 188/62 I_D/I_G = 2.10 $x_c(D)$ = 1 381.9 $x_c(G)$ = 1 557.3 $FWHM_G$ = 146.5	Coating 220/40 I_D/I_G = 2.54 $x_c(D)$ = 1 388.3 $x_c(G)$ = 1 566.3 $FWHM_G$ = 135.9
$\Phi(C_2H_2)+\Phi(Ar)$ = 300 sccm	Coating 150/150 I_D/I_G = 3.95 $x_c(D)$ = 1 381.8 $x_c(G)$ = 1 580.7 $FWHM_G$ = 103.9	-	Coating 250/50 I_D/I_G = 2.74 $x_c(D)$ = 1 390.7 $x_c(G)$ = 1 569.0 $FWHM_G$ = 124.9

Figure 8 shows the relationship between the Raman parameter and mechanical properties. As mentioned before, the configuration of chain used to estimation of the sp^3 bonds presence and contributes to higher hardness. In Figure 8 a) the coatings with I_D/I_G that are smaller than 2.0 had relative high HV and E_{IT} due to presence of sp^3 bonds. The coatings with I_D/I_G from 2.0 to 4.0 had generally lower HV and E_{IT}. A propetional relationship is here not very pronounced. According to [34], the FWHM of the G peak and the sp^2 grain size have a logarithms proportional relationship. The higher the FWHM values of G peak, the finer the sp^2 grain

size. For example in Figure 8, the Raman spectra of coating 150/150 with $FWHM_G$=103.90 cm^{-1} indicates that the sp^2 grain size in this coating is around 2 to 3 nm. In contrast, the coating 166/34 has a sp^2 grain size in the range of about 0.8-0.9 nm. According to [28] and [30], the a-C:H is described as a carbon network with large amount of small sp^2 clusters distributed in it. In this paper, all involved a-C:H variations contain little to rare sp^3 content. Thus, grain size of sp^2 content is key parameter to estimate the coating hardness. In the grain boundary strengthening theory (also Hall-Petch Strengthening), the critical shear strength τ is inversely proportional to grain diameter D: $\tau \propto 1/D^{1/2}$ [35], which can good explain the high hardness of coating 166/34.[1]

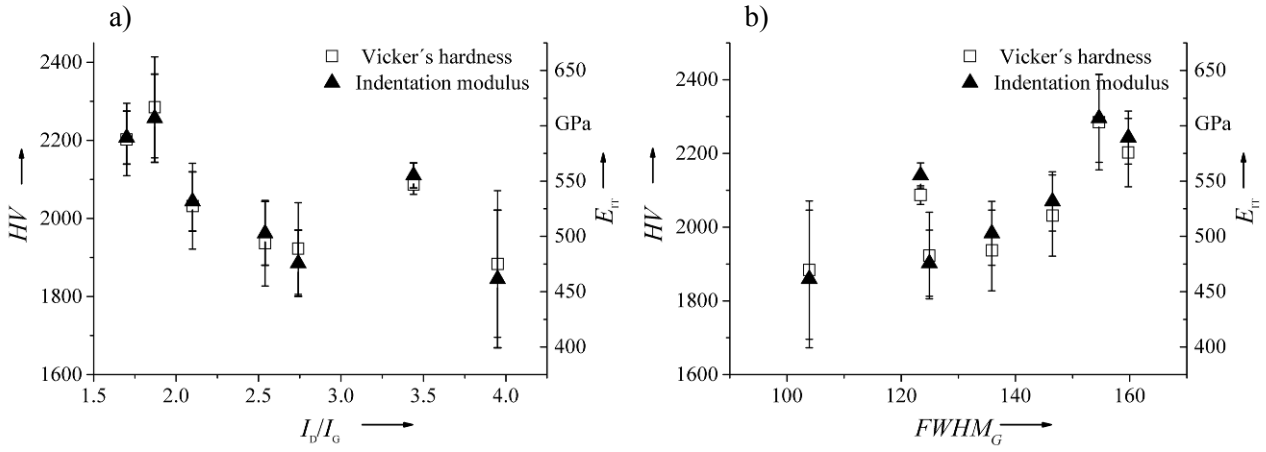

Figure 8: *Variation of Vicker´s hardness HV and indentation modulus E_{IT} with increasing (a) I_D/I_G and (b) FWHM of the G peak.*

3.3 Friction and wear in the ring-on-dics test

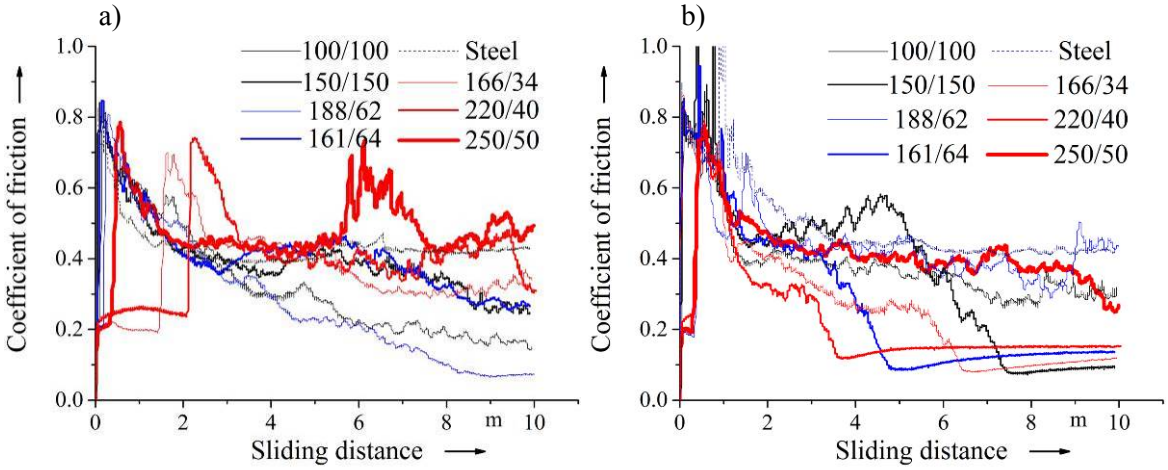

Figure 9: *The variation of the coefficient of friction of all coatings with sliding distance when tested against a) AA5182 and b) AA6014 at 500 N load.*

In Figure 9 one of the three repeated tribological tests was described for each coating variation. Figure 9 a) describes the sliding behaviour of all the coatings against AA5182. As shown in the initial phase of the diagram, coatings 220/40 and 166/34 show unique plateaus with very low coefficients of friction from 0.2 to 0.25. The same plateau appears also for coating 250/50 within the first 0.4 meter sliding distance. The coatings with plateaus in initial phase are deposited under high C_2H_2 concentration. No such plateau was observed for coating deposited under ratios of 1:1 and 3:1. That means these samples were deposited under a relatively high Ar concentration. The Ar gas has surface sputtering effect during the deposition process, especially if the concentration was very high. The high density ion bombardment contributes to increased numbers of the so-called adatoms as well as adsorption sites [19], [26], which may lead to weak bonds [36] or even loose atoms on surface. This makes the coating structure inhomogeneous und thus it takes those coatings longer time to set the stabilized state in terms of surface asperities and possible aluminium transfer.

[1] The Hall-Petch Strengthening is valid for grain size up to 10 nm

After the phase with plateau, aluminium adhesion started to propagate in a not repeatable way, which resulted in unstable and higher coefficient of friction in the diagram. As soon as the aluminium transfer accumulated to a certain height, the a-C:H coating had no more or little contacts to aluminium alloy sheet. Figure 9 b) shows the CoF of all coatings against AA6014. Unlike the CoFs against AA5182, almost none of the coatings show obvious stabile CoF plateau at the beginning of sliding. Some of the coatings, *e.g.* 220/40, 161/64, 166/34 and 150/150, show stable CoFs after 4 to 8 meter sliding distance.
As mentioned before, the appearance of plateau phase at the beginning of sliding are essential and beneficial for forming process. To characterize the appearance of steady plateaus, mean values of CoFs from 0.3 to 0.8 meter are calculated and summarized in Figure 10. Coatings 166/34 and 220/40 against AA5182 show reliable and steady low CoF after three repetitions at the beginning of sliding. The results against AA6014 did not show remarkable difference.

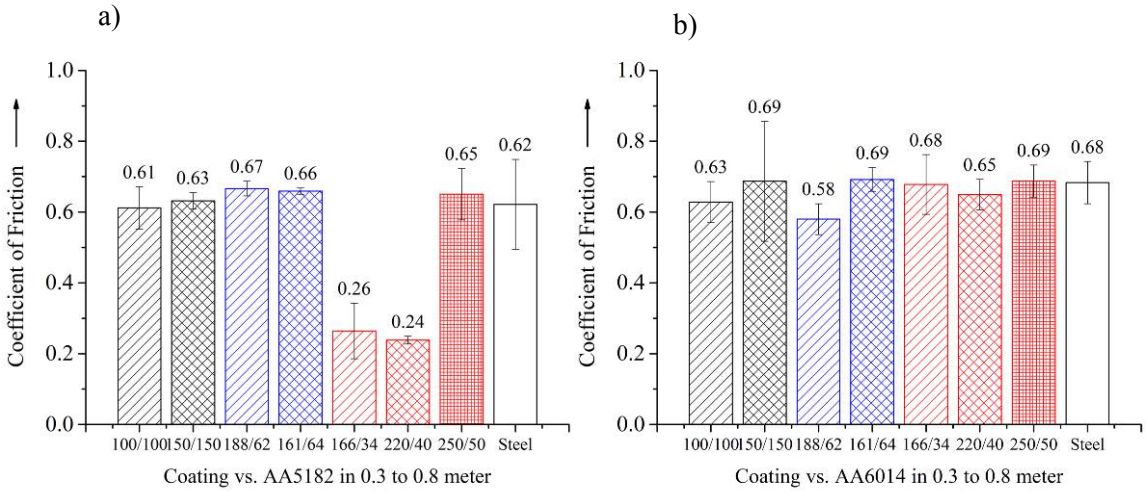

Figure 10: *Mean values of CoFs of all coatings within sliding distance from 0.3 to 0.8 meter when tested against (a) AA5182 and (6) AA6014 at 500 N load.*

As shown in Figure 9, the low friction is often associated with appearance of stable phase. In order to characterise the stable phase, the mean values of CoFs from 9 to 10 meter are summarized in Figure 11. It was noticeable, that CoFs of all coatings against AA5182 show great standard deviations due to adhesive friction. Besides the coating 220/40, the coating 250/50 also showed lower CoF against AA6014.

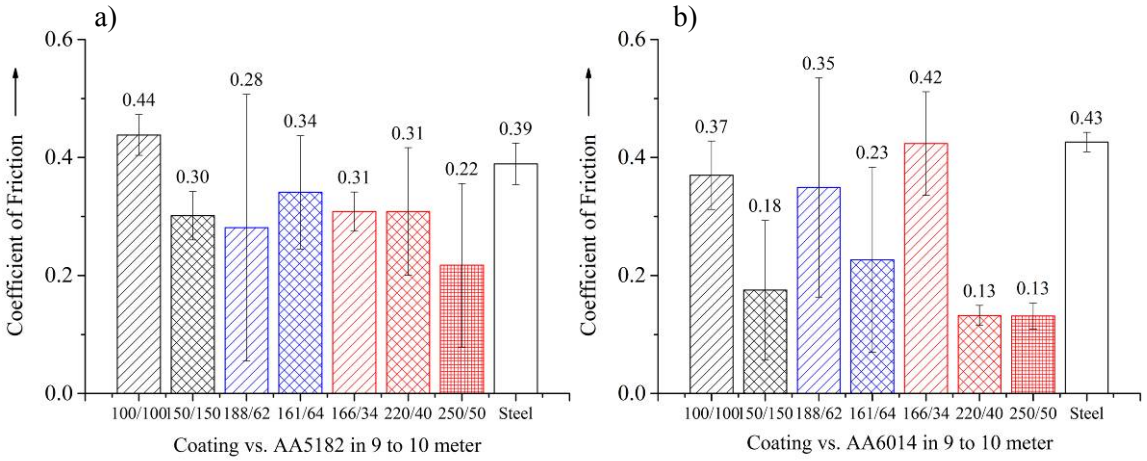

Figure 11: *Mean values of CoFs of all coatings within sliding distance from 9 to 10 meter when tested against (a) AA5182 and (6) AA6014 at 500 N load.*

Figure 12 shows some of the worn ring surfaces. On these worn coating surfaces against AA6014 no visible to little aluminium adhesive wear was observed. It implies that the adhesions are primarily responsible for high and unstable CoF during sliding. In addition, the effect of loose wear particles in this closed tribological system could not be ignored. But the tested ring surfaces can be divided into an inner and an outer ring area,

as shown in Figure 12. Due to the higher velocity compared to that of the inner ring area, the outer area was smoothed and the inner area remained in its original state.

Sheet materials	Coating variation	1st test	2nd test	3rd test
AA5182	166/34			
	220/40			
	250/50			
	150/150			
AA6014	166/34			
	220/40			
	250/50			
	150/150			

Figure 12: *Some of the worn coating surfaces after sliding.*

The worn surfaces were analysed by LSM in the example of 188/62. As shown in Figure 13 a), obvious aluminium adhesion was observed on ring surface. In the inner and outer ring area with no. 1 and 3 very fine wear fragments were detected under microscope. The adhesion ring was analysed and adhesion with a height

of about 5 µm was observed. Figure 13 b) shows the worn coating surface without visible adhesion after testing against AA6014. After testing the ring surface was divided into two areas. The area 3 is smoothed after sliding in comparison to area 1 due to loose wear particle with higher sliding velocity. Considering the transition region between the 2 areas, a height difference of about 0.2 to 0.3 µm was detected.

a) a-C:H Coating 188/62 vs. AA5182

b) a-C:H Coating 188/62 vs. AA6014

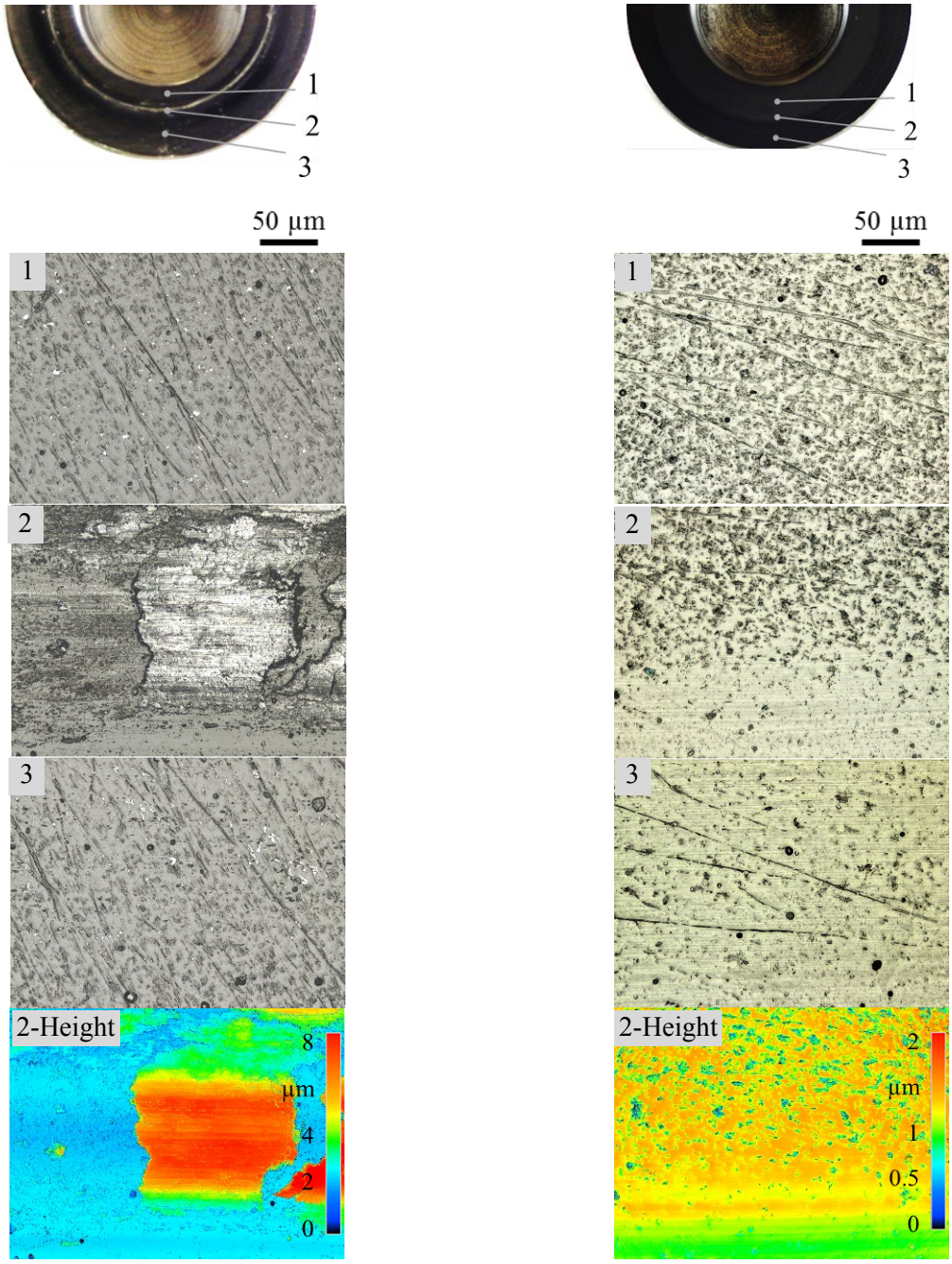

Figure 13: *Wear appearances of worn coating surfaces 188/62 against a) AA5182 and b) AA6014 by laser scanning microscope*

3.4 Friction and wear in strip drawing test

One coating variant is tested under more process like tribological conditions in a flat strip drawing test. The coating parameters are selected by evaluating the friction coefficient of the running-in phase, the average friction coefficient and wear behaviour of the coatings. Comparing the running-in phase for tests with AA6014, the variants 100/100, 188/62 and 220/40 showed a slightly lower friction than the other configuration. However, considering the standard deviation there is no considerable difference. For AA5182 the coating types 166/34 and 220/40 revealed significant lower friction at the running-in phase of 0.25

compared to the other variants with coefficients of friction between 0.61 and 0.67. Additionally, the coating 220/40 revealed a very low deviation which is a sign for more stable tribological conditions. Regarding the average friction in the range between 9 and 10 m sliding distance, the variants 250/50 and 220/40 lead to significantly lower friction compared to other coatings in contact with AA6014. In tests with AA5182, the average coefficient of friction varies in a broad range without significant differences between the coating variants. Comparing the wear tracks for 166/34 and 220/40 in contact with AA5182 in Figure 12, reveals similar wear behaviour for test one and three. In test two, the amount of adhesion for 220/40 is much smaller than for 166/34. For AA6014 the best results in tribometer tests revealed for 250/50 and 220/40. Both depict no macroscopic occurrence of adhesion in Figure 12. In order to compare the tribological properties for both materials with the same variant, coating type 220/40 showed the most beneficial wear behaviour. A beneficial running-in behaviour for AA5182 and very low average friction for AA6014 was observed in ring-on-disc tests. Thus, these coating parameters are used for coating deposition on two pairs of friction jaws. The results of the strip drawing tests for both aluminium alloys are shown in Figure 16. For both materials a reference with metallic bright, uncoated tools was performed. Under dry conditions and without coating the contact pressure needed to be reduced to 2.0 MPa because otherwise high friction would cause cracking of the sheet metal strip especially for AA6014. With coated friction jaws three strips were drawn for each aluminium alloy. The development of coefficient of friction revealed very stable conditions independent of sheet material and strip number. For AA6014 the coefficient of friction is reduced from approximately 0.6 to 0.19. With sheet metal strips out of AA5182 the friction is decreased from 0.24 to 0.19 when an a-C:H coating is applied on the tool surfaces. Thus independent from sheet material friction a constantly lower friction level is achieved.

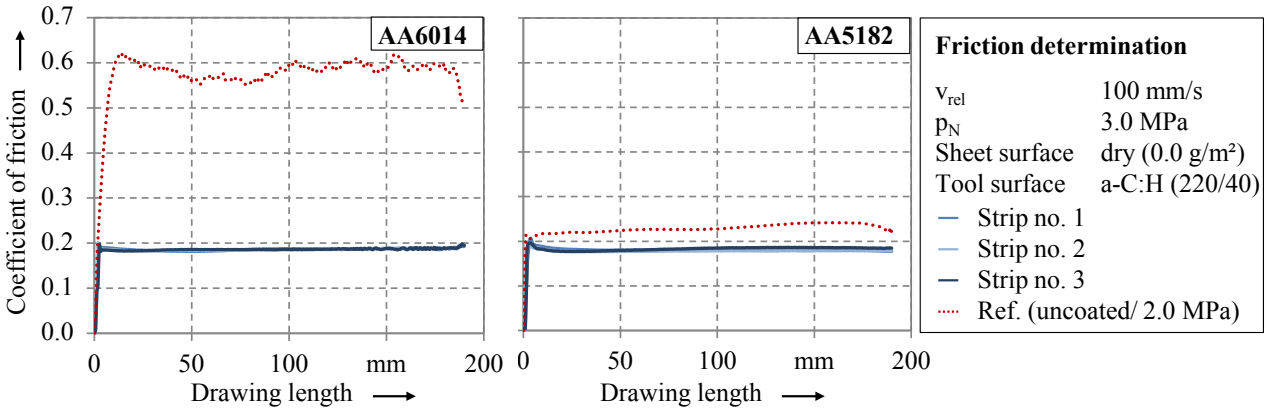

Figure 14: *Determined coefficient of friction for AA6014 and AA5182 in contact with uncoated and a-C:H coated tools.*

Having a closer look at the tool surfaces after strip drawing tests, significant difference reveal for coated and uncoated jaws. Figure 16 presents pictures of the complete contact area and result of confocal microscopy after the experiments. The uncoated jaws reveal adhesive wear for both aluminium alloys. According to the more than two times higher coefficient of friction for AA6014 in contact with uncoated tools, also the amount of adhesion is much higher. The surface analysis for a-C:H coated friction jaws reveal no visible signs of wear neither on a macroscopic nor on a microscopic scale.

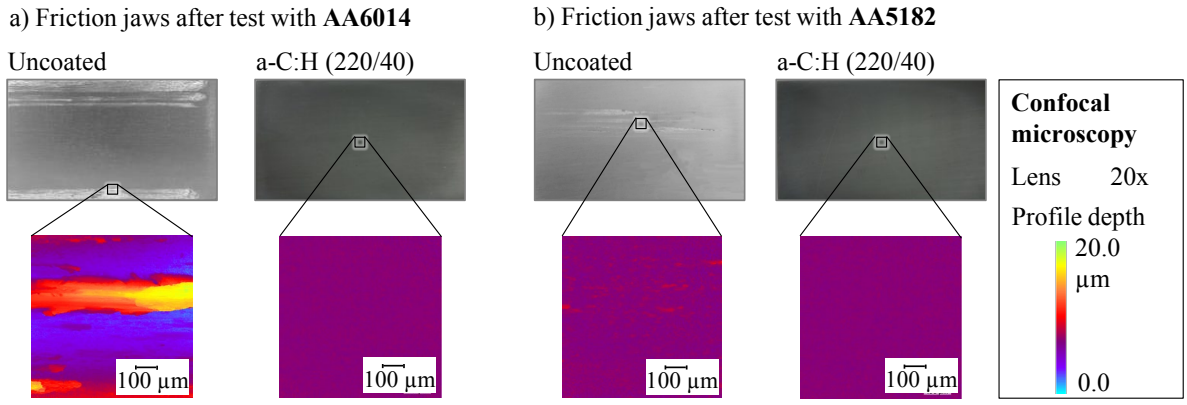

Figure 15: *Surface analysis of friction jaws after strips drawing tests.*

Overall, the results of flat strip drawing tests revealed a promising tribological behaviour of a-C:H coated jaws in contrast to uncoated tools. Friction is reduced to a low and stable level for both aluminium alloys. Furthermore, the occurrence of adhesion is prevented successfully when an a-C:H top layer is applied.

4. CONCLUSION AND OUTLOOK

Amorphous carbon coatings show great potentials to realize a lubricant-free metal sheet forming process due to its unique atom network. In this work, the influences of process pressure and acetylene concentration in gas atmosphere on coating properties were investigated. Divers a-C:H coatings were deposited on tool steel 1.2379 with similar surface roughness of a normal forming tool. The deposition rate, adhesion, hardness and indentation modulus of a-C:H coatings depend on deposition parameters, especially the total gas flow. The deposition rate increases with total gas flow due to formation of more clusters in the initial coating growth phase. Due to less energetic particles caused by short mean free path in the plasma, hardness und indentation moduli reduce as the total gas flow rises. Raman spectra of all coatings samples show characteristic parameter to identify chemical bonds in the coating samples. All investigated coating samples are described as a mixture of nanocrystalline graphite and a-C:H carbon network. Furthermore, the Raman parameters indicate that sp^2 grain sizes are key parameters to determine their differences in hardness and modulus in case of sp^3-rare coatings. The coating variations behave differently in the simple ring-on-disc-tribometer. Some of the coating variations show low CoFs in initial phase and steady phase. Coatings deposited under high acetylene concentration are found to have a clear characteristic plateau with low CoF to about 0.2 against AA5182 in the initial phase of tribological test. The same plateaus were also observed against AA6014 only for a short period of time. Coatings with this feature behave very beneficial in the process-like strip draw test. The selected coating 220/40 shows significantly reduction of CoF and adhesion in comparison to uncoated tool steel. The dominated wear mechanism against aluminium alloys is adhesion. The adhesive friction results in unstable dry sliding. The application of a-C:H coatings can reduce effectively adhesion transferred from workpiece. In this way, the a-C:H coatings can be seen to have great potential to solve tribological problems during lubricant-free sliding process. In the next step, the questions like, if there is a tribochemical film and to detect this film formed by DLC with OH-group using transmission electron microscope, should be answered. Negative effects in the closed ring-on-disc tribosystem were observed, *e.g.* remained loose wear particles between tool/workpiece and thus increased sliding temperature because the same surface was always in contact. Thus, an open tribometer rig with smaller contact area but the same contact pressure is desired.

5. ACKNOWLEDGMENT

The authors thank the German Research Foundation (DFG) for supporting the presented investigations by funding project TR 1043/1-1 and ME 2043/43-1 as part of the priority program SPP 1676 (Dry Metal Forming). Furthermore the authors thank Mr. Dr. S. Jäger from Bavarian Center for Applied Energy Research for his help to conduct Raman measurements and student assistant Mr. S. Frühwald for supporting the tribological experiments.

6. REFERENCE

1. F. Vollertsen, F. Schmidt, Dry Metal Forming: Definition, Chances and Challenges. International Journal of Precision Engineering and Manufacturing. 1(1) (2014) 59-62.
2. K.-H. Habig, Verschleiß und Härte von Werkstoffen, Hanzer, Munich, 1980.
3. H. Czichos, Tribologie-Handbuch, Tribometrie, Tribomaterialien, Tribotechnik, 4th ed., Springer Fachmedien Wiesbaden, Wiesbaden, 2015.
4. R. Woska, J. Barbehön, Metallische Adhäsion unter trockener Reibung, Zeitschrift für Werkstofftechnik. 13 (1982) 348-355.
5. F.P. Bowden, D. Tabor, The Friction and Lubrication of Solids, Part 1, Part 2, Oxford Clarendon Press, UK, 1950, 1964.
6. K. Bewilogua, C.V. Cooper, C. Specht, J. Schröder, R. Wittorf, M. Grischke, Effect of target material on deposition and properties of metal-containing DLC (Me-DLC) coatings. Surface and Coating Technology, 132(2-3) (2000) 275-283.

7. H. Hetzner, C. Schmid, S. Tremmel, K. Durst, S. Wartzack, Empirical-Statistical Study on the Relationship between Deposition Parameters, Process Variables, Deposition Rate and Mechanical Properties of a C:H:W. Coatings. 4(4) (2014) 772-795.
8. M. Merklein, M. Schmidt, S. Tremmel, S. Wartzack, K. Andreas, T. Häfner, R. Zhao, J. Steiner, Investigation of Tribological Systems for Dry Deep Drawing by Tailored Surfaces, Dry Metal Forming - OAJ FMT. 1 (2015).
9. A. Ghiotti, S. Bruschi, Tribological Behaviour of DLC Coatings for Sheet Metal Forming Tools, Wear. 271(9-10) 2011, 2454-2458.
10. M. Murakawa, N. Koga, T. Kumagai, Deep-drawing of aluminium sheets without lubricant by use of diamond-like carbon coated dies, Surface and Coating Technology. 76-77 (1995) 553-558.
11. S. Bhowmick, A. Banerji, M.Z.U. Khan, M.J. Lukitsch, A.T. Alpas, High temperature tribological behavior of tetrahedral amorphous carbon (ta-C) and fluorinated ta-C coatings against aluminum alloys, Surface and Coating Technology. 284 (2015) 14-25.
12. J. Wang, Z. Cao, F. Pan, F. Wang, A. Liang, J. Zhang, Tuning of the microstructure, mechanical and tribological properties of a-C:H films by bias voltage of high frequency unipolar pulse, Applied Surface Science. 356 (2015) 695-700.
13. W. Tillmann, F. Hoffmann, S. Momeni, R. Heller, Hydrogen quantification of magnetron sputtered hydrogenated amorphous carbon (a-C:H) coatings produced at various bias voltages and their tribological behavior under different humidity levels, Surface & Coatings Technology, 206 (2011) 1705–1710
14. Y. Pauleau, Residual Stresses in DLC Films and Adhesion to Various Substrates. In: C. Donnet, A. Erdemir, Tribology of Diamond-Like Carbon Films. Springer, New York, 2008.
15. S. Sattel, J. Robertson, H. Ehrhardt, Effects of deposition temperature on the properties of hydrogenated tetrahedral amorphous carbon, Journal of Applied Physics. 82 (1997) 4566-4576.
16. A. N. Fadzilah, M. Rusop, Effect of deposition temperature of amorphous carbon thin films, in: International Conference on Electronic Devices, Systems and Applications (ICEDSA), Kuala Lumpur, Malaysia, 2011, 328-332.
17. N.M.S. Marinsa, R.P. Mota, R.Y. Honda, P.A.P. Nascente, M.E. Kayama, K.G. Kostov, M.A. Algatti, N.C. Cruz, E.C. Rangel, Properties of hydrogenated amorphous carbon films deposited by PECVD and modified by SF6 plasma, Surface and Coatings Technology, 206 (2011) 640-645.
18. R. Zhao, S. Tremmel. PVD-/PECVD-DLC Thin Coatings as a Potential Solution for Tailored Friction Conditions for Dry Sheet Metal Forming Tools, in: Proceedings of the 12th THE A Coating, Hannover, Germany, 2016, in press.
19. G. Capote, G.C. Mastrapa, V.J. Trava-Airoldi, Influence of acetylene precursor diluted with argon on the microstructure and the mechanical and tribological properties of a-C:H films deposited via the modified pulsed-DC PECVD method, Surface and Coating Technology. 284 (2015) 145-152.
20. German Institute for Standardization (DIN) DIN EN ISO 4287, Beuth, Berlin, 2010.
21. German Institute for Standardization (DIN) DIN EN 1071, Beuth, Berlin, 2003.
22. German Institute for Standardization (DIN) DIN EN ISO 14577, Beuth, Berlin, 2003.
23. S. Prawer, K.W. Nugent, Y. Lifshitz, G.D. Lempert, E. Grossman, J. Kulik, I. Avigal, R. Kalish, Systematic variation of the Raman spectra of DLC films as a function of sp2:sp3 composition, Diamond and Related Materials. 5(3-5) (1996) 433-438.
24. A. Birkert, S. Haage, M. Straub, Umformtechnische Herstellung komplexer Karosserieteile, Auslegung von Ziehanlagen, Springer Vieweg, Berlin, 2013.
25. W. Kleppmann, Taschenbuch Versuchsplanung. Produkte und Prozesse optimieren, 7th ed., Hanzer, Munich, 2011.
26. J. Roberson, Diamond like amorphous carbon, Material Science Engineering Review. 37(4-6) (2002) 129-281.
27. B.R. Pujada, G.C.A.M. Janssen, Density, stress, hardness and reduced Young´s modulus of W-C:H coatings, Surface and Coating Technology. 201 (2006) 4284-4288.
28. H. Hetzner, Systematische Entwicklung amorpher Kohlenstoffschichten unter Berücksichtigung der Anforderungen der Blechmassivumformung. Dissertation. Nuremberg, 2014.
29. B. Rother, J. Vetter, Plasma-Beschichtungsverfahren und Hartstoffschichten, deutsche Verlag für Grundstoffindustrie, Leipzig, 1992.
30. H.-G. Fuss, M. Frank, Industrial Production of DLC Coatings. In: C. Donnet, A. Erdemir, Tribology of Diamond-Like Carbon Films. Springer, New York, 2008.

31. M. Rigolio, C. Castiglioni, G. Zerbi, F. Negri, Density functional theory prediction of the vibrational spectra of polycyclic aromatic hydrocarbons: effect of molecular symmetry and size on Raman intensities, Journal of Molecular Structure. 563-564 (2001) 79-87.
32. A. C. Ferrari, J. Robertson, Resonant Raman spectroscopy of disordered amorphous, and diamond-like carbon, Physical Review B. 64(7) (2001) 075414.
33. A. C. Ferrari, J. Robertson, Interpretation of Raman spectra of disordered and amorphous carbon, Physical Review B. 61(20) (2000) 14095.
34. A. C. Ferrari, S. E. Rodil, J. Robertson, Interpretation of infrared and Raman spectra of amorphous carbon nitrides, Physical Review B. 67 (2003) 155306.
35. G. Gottstein, Materialwissenschaft und Werkstofftechnik, Physikalische Grundlagen, 4th. ed., Springer Vieweg, Berlin, 2014, 266-268.
36. K. Bobzin, Oberflächentechnik für den Maschinenbau. 1st ed., Wiley-VCH Verlag, Weinheim, 2013.